A&A 652, A15 (2021)
https://doi.org/10.1051/0004-6361/202140828

Astronomy & Astrophysics

Long-term X-ray evolution of SDSS J134244.4+053056.1

A more than 18 year-old, long-lived IMBH-TDE candidate

J. S. He[1], L. M. Dou[1], Y. L. Ai[2,6], X. W. Shu[3], N. Jiang[4], T. G. Wang[4], F. B. Zhang[3], and R. F. Shen[5]

[1] Department of Astronomy, Guangzhou University, Guangzhou 510006, PR China
e-mail: doulm@gzhu.edu.cn
[2] College of Engineering Physics, Shenzhen Technology University, Shenzhen 518118, PR China
[3] Department of Physics, Anhui Normal University, Wuhu, Anhui 241000, PR China
[4] CAS Key Laboratory for Researches in Galaxies and Cosmology, Department of Astronomy, University of Science and Technology of China, Hefei, Anhui 230026, PR China
[5] School of Physics and Astronomy, Sun Yat-Sen University, Zhuhai 519082, PR China
[6] Shenzhen Key Laboratory of Ultraintense Laser and Advanced Material Technology, Shenzhen 518118, PR China

Received 18 March 2021 / Accepted 21 May 2021

ABSTRACT

SDSS J134244.4+053056 is a tidal disruption event candidate with strong temporal coronal line emitters and a long fading, mid-infrared dust echo. We present detailed analyses of X-ray emission from a *Swift*/XRT observation in 2009 and the most recent *XMM-Newton*/pn observation in 2020. The two spectra can be modeled with hard and soft components. While no significant variability is detected in the hard component above 2 keV between these two observations, the soft X-ray emission in 0.3–2 keV varies by a factor of ∼5. The luminosity of this soft component fades from $\sim 1.8 \times 10^{41}$ to $\sim 3.7 \times 10^{40}$ erg s^{-1} from the observation in *Swift* to that of *XMM-Newton*, which are 8 and 19 years after the outburst occurred, respectively. The evolution of luminosity matches with the $t^{-5/3}$decline law well; there is a soft X-ray peak luminosity of 10^{44} erg s^{-1} at the time of the optical flare. Furthermore, the spectra of the soft component harden slightly in the decay phase, in which the photon index Γ varies from $4.8^{+1.2}_{-0.9}$ to 3.7 ± 0.5, although they are consistent with each other if we consider the uncertainties. Additionally, by comparing the BH mass estimate between the $M - \sigma$ correlation, the broad Hα emission, and the fundamental plane relation of BH accretion, we find that a value of $\sim 10^5$ $M_\odot$ is favored. If so, taking its X-ray spectral variation, luminosity evolution, and further support from theory into account, we suggest that SDSS J134244.4+053056 is a long-lived tidal disruption event candidate lasting more than 18 years with an intermediate-mass black hole.

Key words. accretion, accretion disks – black hole physics – X-rays: galaxies – galaxies: individual: SDSS J134244.4+053056.1

1. Introduction

A tidal disruption event (TDE), in which a star passing too close to a supermassive black hole (SMBH) in a galactic nucleus is torn apart by the tidal force of the hole, is of particular interest. As a result of a TDE, about half of the stellar debris is accreted by the SMBH, producing a luminous electromagnetic flare (e.g., Rees 1988; Evans & Kochanek 1989). The transient luminosity would follow the same time dependence as the mass fallback rate, which is generally assumed as $t^{-5/3}$. For a Schwarzschild black hole (BH) with $M_{\rm BH} > 10^8\ M_\odot$ the tidal disruption radius of a solar-type star is in the event horizon and no electromagnetic flare would be observed (Hills 1975).

The first TDE candidate was discovered in the soft X-ray band by the ROSAT all-sky survey in the 1990s and can be well interpreted by the TDE scenario (Bade et al. 1996; Komossa & Bade 1999). The general picture for soft X-ray TDEs is that at first the flare is up to several 10^{44} erg s^{-1} in soft X-ray band with an Eddington accretion rate. Then, the luminosity declines on a timescale of months to years. Finally, the hardening of X-ray spectra indicates that the disk and corona coexist on the phase with a low accretion rate (Komossa 2015; Saxton et al. 2020). Approximately 20 soft X-ray TDEs have been discovered until now (see the review in Saxton et al. 2020).

As a consequence of the rapid development of time-domain astronomy in recent years, especially large optical sky surveys, the number of TDEs has increased to ∼100. Most of these have been discovered in the optical band, and many of the optical TDEs have no or weak X-ray detection in their very early phases during the outbursts. However, X-ray emissions have been detected in three out of four optically discovered TDEs about four to nine years after the optical flares, and most TDEs have been suggested as bright X-ray sources visible for at least a decade (Jonker et al. 2020). Therefore, research in the X-ray band is still one of the most important tools for identifying and studying TDEs.

In the gas-rich environment, the extreme ultraviolet (EUV) X-ray emission from TDEs can photoionize the surrounding gas, thereby producing luminous, transient high-ionization coronal emission lines (e.g., Komossa et al. 2008; Wang et al. 2011, 2012). While in a dust-rich environment, high-energy X-ray photons from the TDEs are absorbed by dust and then reradiated in the infrared band (Lu et al. 2016). Such light echoes have been observed in the mid-infrared light curves of some TDEs (Dou et al. 2016, 2017; Jiang et al. 2016, 2017, 2019; van Velzen et al. 2016) and used as an efficient method to search for TDE candidates (Wang et al. 2018; Jiang et al. 2021).

SDSS J134244.4+053056 (hereafter J1342) is a TDE candidate with transient extreme optical coronal emission lines at a redshift of 0.0366. Strong high ionization coronal lines appeared in a SDSS spectrum (e.g., [Fe X], [Fe XI] and [Fe XIV]) on April 09, 2002, but disappeared in the following multiple mirror

Table 1. Log of the X-ray observations.

(1) Tel./instr.	(2) Obs. ID	(3) Obs. date	(4) Exp. time [ks]	(5) Count rate (soft band) [10^{-3} ct s^{-1}]	(6) Count rate (full band) [10^{-3} ct s^{-1}]
Swift/XRT	00090102001	2009 May 15	6.73	0.80 ± 0.42	1.16 ± 0.52
Swift/XRT	00090102002	2009 May 17	6.60	2.38 ± 0.64	2.61 ± 0.69
Swift/XRT	00090102003	2009 May 20	3.26	0.56 ± 0.53	0.56 ± 0.53
Swift/XRT	Stacking	2009 May 15–20	16.60	1.38 ± 0.32	1.54 ± 0.36
XMM-Newton/pn	0843440201	2020 January 8	12.46	9.3 ± 1.1	10.9 ± 1.2

Notes. Column (1), Telescope and instrument; Cols. (2) and (3), Observation ID and date; Col. (4), Effective exposure time; Col. (5), Count rate in soft X-ray band (0.3–2 keV for *Swift*/XRT and 0.2–2 keV for *XMM-Newton*/pn); Col. (6) Count rate in full X-ray band (0.3–10 keV for *Swift*/XRT and 0.2–10 keV for *XMM-Newton*/pn).

telescope (MMT) spectrum on December 26, 2011 (Wang et al. 2012; Yang et al. 2013). The long-fading mid-infrared emission was also detected in J1342, which was interpreted as an infrared echo from dust in the nuclear region by reprocessing the high-energy radiation of the TDE (Dou et al. 2016). Although we do not have good constraints on the date for its continuum flare, the high-ionization iron coronal lines disappeared in subsequent observations; this suggested that they must be short lived. Thus, the tidal disruption flare happened not too far from the SDSS spectroscopic observation. The peak of the flare is then roughly estimated to occur roughly one year before the SDSS optical spectral observation (see the details in Dou et al. 2016).

Soft X-ray emission was detected in J1342 with *Swift*/XRT observations in May 2009, and this source was classified as a veiled X-ray TDE (Auchettl et al. 2017). However, Chilingarian et al. (2018) argue that the detected X-ray emission was not from a TDE because the observations took place seven years after the time of the speculated optical flare, and these authors attributed the X-ray emission to active galactic nucleus (AGN) activity. Thus, the nature of its X-ray emission is not yet clear. In this paper, with the latest *XMM-Newton* observation in 2020 and the radio observation with VLA in 2016, we present a detailed X-ray and radio analysis of J1342. In Sect. 2, we describe the observations and data reductions. In Sect. 3, we present our results of X-ray spectral fitting and discuss the observed properties in AGN and TDE scenarios, respectively. We conclude in Sect. 4. Throughout this paper, we adopt a standard flat cosmology with $\Omega_M = 0.3$, $\Omega_\Lambda = 0.7$, and a Hubble constant of $H_0 = 70\,\mathrm{km\,s^{-1}\,Mpc^{-1}}$, which results in a luminosity distance of 161.1 Mpc.

2. Data reduction and analysis

2.1. X-ray data reduction

Three observations of J1342 were taken with the X-Ray Telescope (XRT; Burrows et al. 2005) at the *Neil Gehrels Swift* Observatory (*Swift*; Gehrels et al. 2004) during May 15–20 2009. We reduced the data following the standard XRT data reduction[1] with the tools in HEASOFT (v6.26.1). The cleaned events files were reprocessed using the task XRTPIPELINE. Only observations with a "photon counting" mode were used. The source spectrum was extracted from a circular region with radius of 47.2″ at the optical center with the tool XSELECT. The background spectrum was extracted from a larger source-free region near the source. No significant variation was detected among the observations and we stacked the three observations to increase the signal-to-noise ratio (S/N). The net count rate of the target is 0.00139 ± 0.00033, 0.00016 ± 0.00016, and $0.00154 \pm 0.00036\,\mathrm{cts\,s^{-1}}$ in the 0.3–2, 2–10, and 0.3–10 keV bands, respectively.

J1342 was observed with *XMM-Newton* on January 8, 2020 (ObsID: 0843440201; PI: Chilingarian). We reprocessed the *XMM-Newton* data with Science Analysis Software (SAS, v19.0) and the latest calibration files (updated to 2020 July). We only used data from the pn instrument of European Photon Imaging Camera (EPIC-pn) in our analysis considering its high sensitivity and large effective area. The events file was created by 'epchain'. After removing the 'bad' (e.g., hot, dead, or flickering) pixels, the high flaring particle background time interval was created by applying a threshold rate of $>0.5\,\mathrm{cts\,s^{-1}}$ with single events (PATTERN=0) in the 10–12 keV band for EPIC-pn. This results in a net exposure time of 12.46 ks, after removing the high flaring particle background time interval. Only single and double events (PATTERN<=4, FLAG=0) were used for the following analysis. The source spectrum was extracted from a circular region with radius of 20″ centered on its optical position, and the background spectrum was extracted from a nearby source-free circular region with radius of 30″. The net count rate is 0.0093 ± 0.0011, 0.0016 ± 0.0006, and $0.0109 \pm 0.0012\,\mathrm{cts\,s^{-1}}$ in the 0.2–2, 2–10, and 0.2–10 keV bands, respectively.

The logs of *Swift*/XRT and *XMM-Newton*/pn observations are listed in Table 1. The hardness ratio (HR) between 0.3–2 and 2–10 keV[2] is $-0.83^{+0.09}_{-0.17}$ for the stacked *Swift*/XRT observation, and $-0.65^{+0.12}_{-0.12}$ for the *XMM-Newton*/pn observation, which is calculated by the Bayesian estimation of hardness ratios code (BEHR; Park et al. 2006). The values of hardness ratios indicate a slight spectral shape variation between *Swift* and *XMM-Newton* observations, although they are consistent with each other if considering the uncertainties. The *Swift*/XRT stacking spectrum (*Swift* spectrum, hereafter) is then regrouped to have at least three counts per bin, while the *XMM-Newton*/pn spectrum (*XMM-Newton* spectrum, hereafter) is regrouped to least seven counts per bin to adopt the C-statistic for spectral fitting in XSPEC (v. 12.9.1). During the spectral fitting, the uncertainties are estimated at 68% confidence level for one interesting parameter.

[1] http://swift.gsfc.nasa.gov/analysis/xrt_swguide_v1_2.pdf

[2] The hardness ratio is defined as HR = (H − S)/(H + S), where S and H are the source counts for the soft (0.3–2 keV) and hard (2–10 keV) bands.

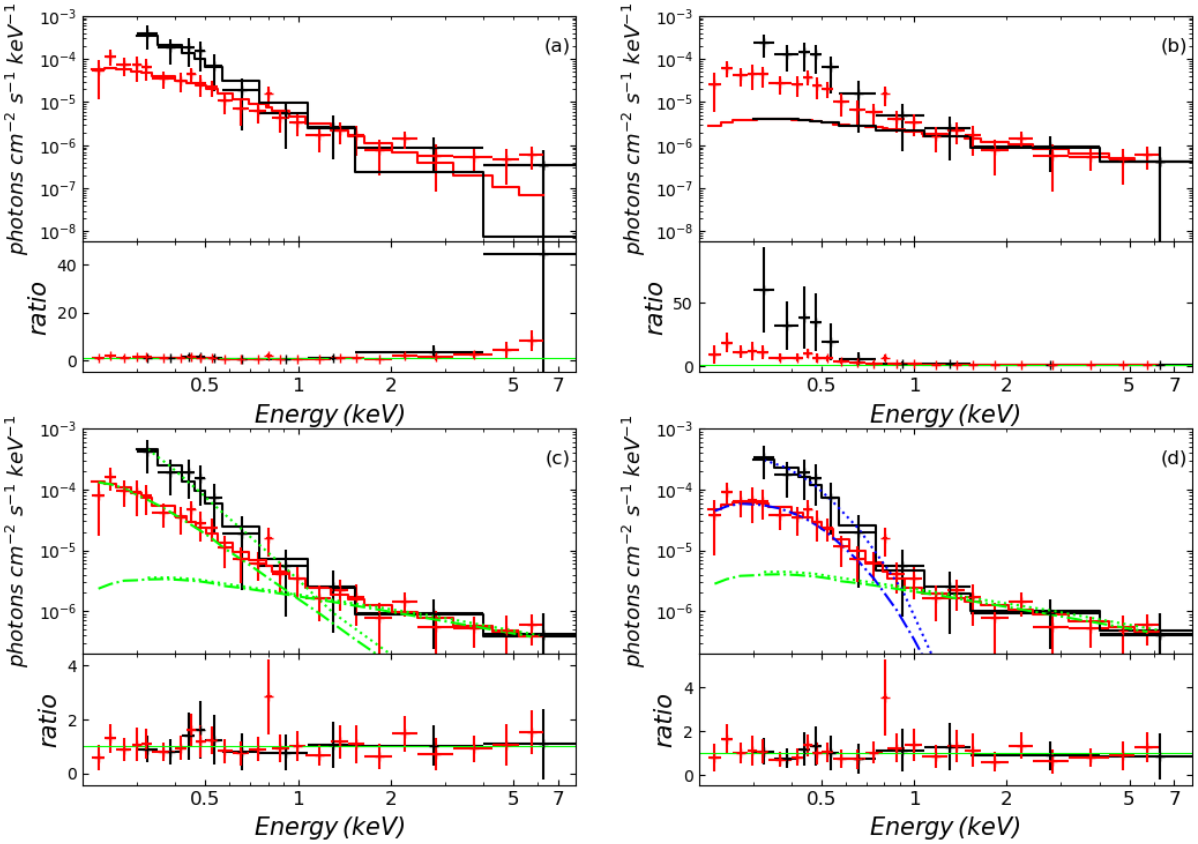

Fig. 1. Unfolded *Swift*/XRT and *XMM-Newton*/pn spectra with fitting model. *Panel a*: a simple PL model is applied to the full band spectrum of *Swift* (0.3–10 keV, black) and *XMM-Newton* (0.2–10 keV, red), respectively. *Panel b*: a simple PL model with fixed photon index at $\Gamma = 0.9$ is applied to the 1–10 keV band and extended to the full band spectrum of *Swift* and *XMM-Newton*, respectively. *Panel c*: PL+PL model with fixed photon index at $\Gamma = 0.9$ for one PL component is applied to the full band spectrum of *Swift* and *XMM-Newton*, respectively. *Panel d*: PL+BB model with one fixed photon index at $\Gamma = 0.9$ for the PL component is applied to the full band spectrum of *Swift* and *XMM-Newton*, respectively. The data/model ratio is also shown in each panel.

2.2. X-ray spectral analysis

First, a simple Galactic absorbed power-law model (PL) with column density fixed at the Galactic value of 1.82×10^{20} cm^{-2} (Kalberla et al. 2005, the Galactic absorption is included in all following spectral fitting) is applied to the *Swift* and *XMM-Newton* spectrum, respectively. The inferred photon index is $\Gamma = 3.9^{+0.8}_{-0.6}$ for *Swift* spectrum (C-statistic/d.o.f. = 3.8/8) and $\Gamma = 2.4 \pm 0.3$ for *XMM-Newton* spectrum (C-statistic/d.o.f. = 19.5/25). However, the residuals in the hard 2–10 keV band in both of the two spectra indicate that the other component is needed to well represent the data, as shown in Fig. 1a. The PL model is then applied to the *XMM-Newton* 1–10 keV spectrum because the S/N is better than that of *Swift*. The inferred photon index is $\Gamma = 0.9^{+0.4}_{-0.4}$ (C-statistic/d.o.f. = 2.1/7). We then extrapolated this model to the whole 0.3–10 keV (0.2–10 keV) band spectrum of *Swift* (*XMM-Newton*). As shown in Fig. 1b, there are significant excesses in soft X-ray band, especially for the *Swift* spectrum.

So we applied the two PL model to the spectra with one photon index fixed at 0.9. The fitting is acceptable and the inferred photon index of the soft PL component is $\Gamma = 3.7 \pm 0.5$ for the *XMM-Newton* spectrum and $\Gamma = 4.8^{+1.2}_{-0.9}$ for the *Swift* spectrum. The soft PL component for the *Swift* spectrum is slightly steeper than that of *XMM-Newton*, although there is no significant difference considering the uncertainties. But the flux is significantly different (Fig. 1c). The flux in 0.3–2 keV of the soft PL component is $5.11^{+0.91}_{-2.22} \times 10^{-14}$ and $1.14^{+0.12}_{-0.15} \times 10^{-14}$ erg cm^{-2} s^{-1}, for *Swift* and *XMM-Newton*, respectively. Notably, there is no flux variation of the hard PL component between the *Swift* and *XMM-Newton* observation. The flux in 2–10 keV of the hard PL component is $2.99^{+2.54}_{-1.13} \times 10^{-14}$ and $2.80^{+0.76}_{-0.61} \times 10^{-14}$ erg cm^{-2} s^{-1} for *Swift* and *XMM-Newton*, respectively.

Since most of the X-ray-selected TDEs can be well fitted with a blackbody model for their soft X-ray band, we used a blackbody (BB) component instead of the soft PL component fitting the spectra (Fig. 1d). The inferred temperature is $kT = 78^{+20}_{-17}$ and $kT = 90^{+16}_{-14}$ eV for *Swift* and *XMM-Newton* spectrum, respectively. The best fitting parameters, including the total fluxes and luminosities in 0.3–2 and 2–10 keV for each model, are listed in Table 2.

2.3. Radio data reduction

J1342 was observed at *C* band (central frequency of 5.5 GHz) with the VLA in its moderately compact C configuration on March 12, 2016 (program code, 15B-247; PI: Zauderer). The data were reduced following standard procedures with the CASA package. Flux density calibration was conducted using 3C286, whereas the nearby source J1347+1217 was used to determine the complex gain solutions, which were interpolated to J1342. After removing the radio frequency interference, the data were imaged using the CLEAN algorithm with Briggs weighting and

Table 2. X-ray spectral fitting results of *Swift*/XRT and *XMM-Newton*/pn spectra.

(1) Model	(2) Γ	(3) Γ_1	(4) kT [eV]	(5) C-s/d.o.f.	(6) $F_{0.3-2\,\mathrm{keV}}$ 10^{-14} [erg cm^{-2} s^{-1}]	(7) $F_{2-10\,\mathrm{keV}}$ 10^{-14} [erg cm^{-2} s^{-1}]	(8) $L_{0.3-2\,\mathrm{keV}}$ 10^{41} [erg s^{-1}]	(9) $L_{2-10\,\mathrm{keV}}$ 10^{41} [erg s^{-1}]
Swift/XRT (0.3–10 keV)								
PL	$3.9^{+0.8}_{-0.6}$			3.81/8	$5.23^{+1.20}_{-1.46}$	$0.14^{+0.01}_{-0.06}$	$1.74^{+0.40}_{-0.49}$	$0.05^{+0.004}_{-0.020}$
PL+PL	$4.8^{+1.2}_{-0.9}$	0.9(fix)		1.17/6	$5.65^{+1.01}_{-2.46}$	$3.01^{+2.56}_{-1.14}$	$1.92^{+0.38}_{-0.77}$	$0.90^{+0.77}_{-0.34}$
PL+BB		0.9(fix)	78^{+20}_{-17}	0.75/6	$5.11^{+0.81}_{-2.25}$	$3.71^{+1.86}_{-1.50}$	$1.67^{+0.26}_{-0.74}$	$1.11^{+0.56}_{-0.45}$
XMM-Newton/pn (1–10 keV)								
PL		$0.9^{+0.4}_{-0.4}$		2.12/7		$3.32^{+1.11}_{-1.30}$		$0.94^{+0.31}_{-0.37}$
XMM-Newton/pn (0.2–10 keV)								
PL	$2.4^{+0.3}_{-0.3}$			19.54/25	$1.65^{+0.20}_{-0.17}$	$0.67^{+0.13}_{-0.33}$	$0.52^{+0.06}_{-0.05}$	$0.22^{+0.04}_{-0.11}$
PL+PL	$3.7^{+0.5}_{-0.5}$	0.9(fix)		8.57/22	$1.64^{+0.17}_{-0.22}$	$2.84^{+0.77}_{-0.62}$	$0.52^{+0.05}_{-0.07}$	$0.85^{+0.23}_{-0.19}$
PL+BB		0.9(fix)	90^{+16}_{-14}	9.13/22	$1.59^{+0.12}_{-0.23}$	$3.35^{+0.66}_{-0.63}$	$0.50^{+0.04}_{-0.07}$	$1.00^{+0.20}_{-0.19}$

Notes. Column (1), Fitting model, PL, PL+PL, and PL+BB are phabs∗powerlaw, phabs∗(powerlaw+powerlaw), and phabs∗(power law+zbbody), respectively, in Xspec; the column density of *phabs* is fixed at the Galactic column density of $N_{\mathrm{H}} = 1.82 \times 10^{20}$ cm^{-2}; Cols. (2)–(3), Photon index Γ of PL component; Col. (4), temperature kT of BB component; Col. (5), best fitting C-statistic/degree of freedom; Cols. (6)–(7), in 0.3–2 and 2–10 keV band after correcting the Galactic absorption; Cols. (8)–(9), luminosity in 0.3–2 and 2–10 keV band after correcting the Galactic absorption.

ROBUST parameter of 0. The final cleaned map has a synthesized beam of 3.2″×2.4″. J1342 is clearly detected as a compact source, with an integrated flux density of 44.9 ± 2.1 μJy, which was measured using the CASA task IMFIT.

3. Discussion

3.1. X-ray origin

The two X-ray spectra can be well described with a two-component model: one component is a hard PL component with photon index of ∼1.0, dominated in the 2–10 keV band; the other is a very soft component as a steep PL with photon index of $\Gamma = 4.8^{+1.2}_{-0.9}$ for *Swift* (or $\Gamma = 3.7 \pm 0.5$ for *XMM-Newton*) or a blackbody with temperature of $kT \sim 70$–90 eV, dominated in the 0.2–2 keV band. In the *Swift* observation, the luminosity of the hard component is ∼1.6 and 8.9×10^{40} erg s^{-1} in 0.3–2 and 2–10 keV, respectively; the soft component is ∼1.8 and 0.008×10^{41} erg s^{-1} in 0.3–2 and 2–10 keV, respectively. In the *XMM-Newton* observation, the luminosity of the hard component is ∼1.5 and 8.4×10^{40} erg s^{-1} in 0.3–2 and 2–10 keV, respectively; the soft component is ∼3.7 and 0.16×10^{40} erg s^{-1} in 0.3–2 and 2–10 keV, respectively.

The host galaxy of J1342 is a star-forming galaxy of which the hot interstellar medium could contribute to X-ray emission. The estimated X-ray emission from its host galaxy is $\sim 5 \times 10^{38}$ erg s^{-1} in 0.3–10 keV using the correlation between the star formation rate (SFR) and the X-ray luminosity (e.g., Mineo et al. 2012), if adopting its SFR of 0.07 $M_\odot$ yr^{-1} (French et al. 2020). This is more than two orders of magnitude lower than the luminosity observed by *Swift* or *XMM-Newton*. Thus, the host galaxy origin for the observed X-ray emission could be ruled out.

The 0.3–2 keV band luminosity of *Swift* observation is ∼3.7 times brighter than that of *XMM-Newton*. If only considering the soft PL component, the luminosity of *Swift* would be ∼4.9 times brighter than that of *XMM-Newton*. However, there is no significant difference in the 2–10 keV band luminosity between *Swift* and *XMM-Newton*. This indicates that the emissions of the soft and hard component may have different origins for J1342.

As the luminosity of the hard component in 0.3–10 keV is 1.0–1.1×10^{41} erg s^{-1} and no significant variation is detected in between the *Swift* and *XMM-Newton* observations, we speculate this component has always existed. The origin of this hard component is unclear. One possibility is that J1342 has some low level of AGN activity. Using the luminosity correlation between $L_{[\mathrm{O\,III}]}$ and L_X in AGNs (e.g., Lamastra et al. 2009), we can also estimate the X-ray contribution of AGN activity from its [O III] narrow emission line. Adopting the [O III] flux of 1.8×10^{-15} erg cm^{-2} s^{-1} (Yang et al. 2013), the estimated 2–10 keV luminosity is 7.5×10^{40} erg s^{-1}, which is consistent with the observed 2–10 keV luminosity of the hard component. This probability is similar to the speculation of Chilingarian et al. (2018).

Soft X-ray excess is a common feature in some AGNs, which is also usually modeled with a blackbody or a steep power law. However, such a steep soft X-ray spectrum is usually detected in X-ray bright AGNs, especially, in NLS1ys (e.g., Ai et al. 2010; Gliozzi & Williams 2020). Additionally, the variability of soft excess is generally concurrent with its disk-coronal emissions in the hard X-ray band. For J1342, the variability is only detected in the soft X-ray band and the observed luminosity is relatively lower than such bright AGNs.

As a TDE candidate with transient coronal lines, variability in the soft X-ray band is expected in J1342. The light curve of 0.3–2 keV band luminosity is shown in Fig. 2. We apply a declined power-law function to fit the light curve as follows:

$$L_{0.3-2\,\mathrm{keV}} = A\,t^{-n},$$

where t is time since the date of the X-ray peak of the tidal disruption flare in unit of year. Here, we adopt the peak of the X-ray flare occurred about one year prior to the SDSS optical spectral observation as estimated in Dou et al. (2016). If we adopt the total X-ray luminosities in 0.3–2 keV band, we obtain a power-law index of $n = 1.6^{+0.2}_{-0.5}$. Fitting to the X-ray luminosity evolution of the soft component in 0.3–2 keV band, we

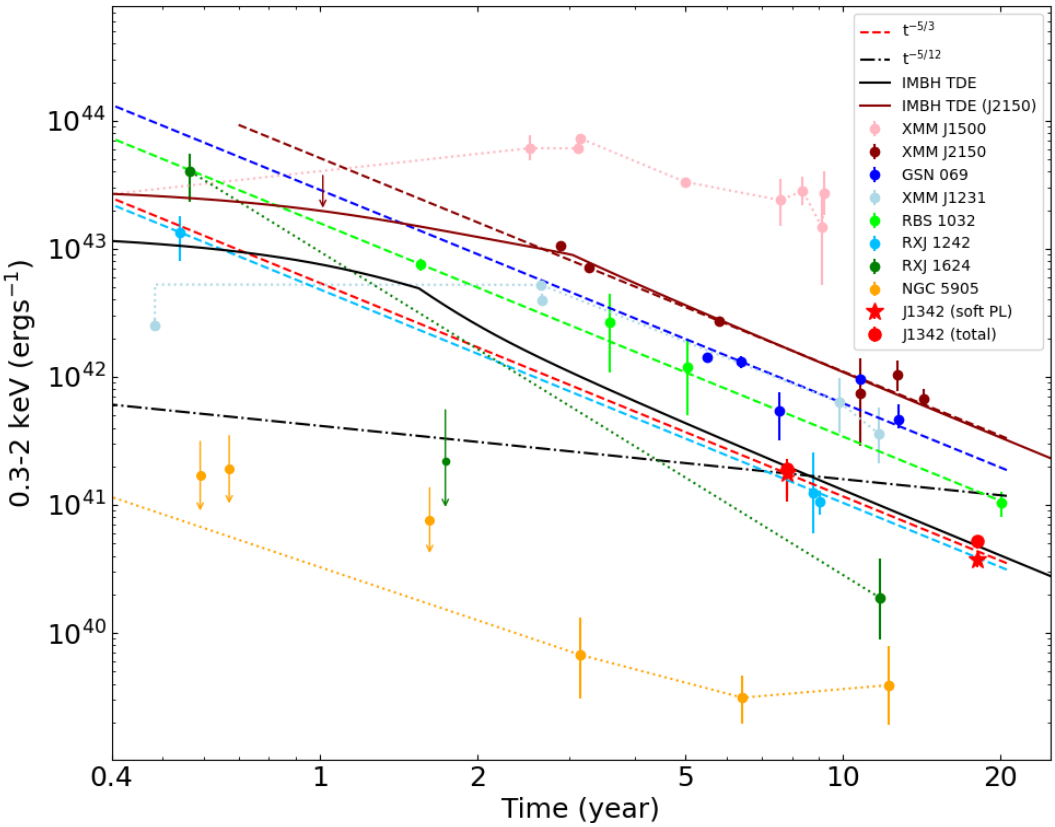

Fig. 2. Later X-ray light curves of TDEs in 0.3-2 keV. The x-axis indicates the time since the flare occurred; for J1342, it is about 1 year before the SDSS optical spectral observation. The total 0.3–2 keV luminosities of J1342 is labeled as a circle symbol; the 0.3–2 keV luminosities of the soft PL component of J1342 is labeled as a pentagram symbol. The later X-ray light curves of other long-lived TDEs are also shown, which include RX J1242.6-1119, RX J1624.9+7554, NGC 5905 (Vaughan et al. 2004), RBS 1032 (Maksym et al. 2014), 3XMM J1500+0154 (Lin et al. 2017a), 3XMM J2150−0551 (Lin et al. 2018, 2020), 2XMM J1231+1106 (Lin et al. 2017b), and GSN 069 (Shu et al. 2018). The luminosities of XMM J1500+0154 are in 0.34–11.5 keV, of RBS 1032 are in 0.1–2.4 keV, and of XMM J2150-0551 are the bolometric luminosities from the disk model; the luminosities of others are converted to those in the 0.3–2 keV band. The later light curves following the power law decline as $t^{-5/3}$ are shown as dashed lines; the others are shown as dotted lines. A power law decline as $t^{-5/12}$ is also shown as a dot-dashed line. The theoretical IMBH-TDE light curve (Chen & Shen 2018) is shown as a solid line.

obtain a power-law index of $n = 1.8^{+0.3}_{-0.5}$. Interestingly, we find the observed X-ray luminosities in 0.3–2 keV well matched the theoretical canonical decline of $t^{-5/3}$ in the fallback model (Rees 1988; Phinney 1989) within errors, although X-ray observations are 8 (*Swift*) and 19 (*XMM-Newton*) years after the outburst (as shown in Fig. 2). In constrat, $t^{-5/12}$ declined power law, predicted with the assumption that the X-ray emissions are from the disk of TDE (e.g., Cannizzo & Gehrels 2009; Lodato & Rossi 2011), deviates from the data. Furthermore, the expected 0.3–2 keV band luminosity peak is at $\sim 10^{44}$ erg s^{-1}, which is also consistent with the luminosity peak in other soft X-ray discovered TDEs (Komossa 2015; Saxton et al. 2020). Additionally, the spectral slope of the soft component of J1342 is $\Gamma = 4.8^{+1.2}_{-0.9}$ for *Swift* and $\Gamma = 3.7 \pm 0.5$ for *XMM-Newton*, or $kT = 78^{+20}_{-17}$ eV for *Swift*, and $kT = 90^{+16}_{-14}$ eV for *XMM-Newton* if modeling with a blackbody.

3.2. Radio origin

J1342 is clearly detected as a compact radio source, with an integrated flux density of 44.9 ± 2.1 μJy at 5.5 GHz. There are three possible origins for the radio emission: star formation, AGN, and/or TDE. If assuming the radio-derived SFR ($\mathrm{SFR_{radio}}$) equal to the optical SFR of 0.07 $M_\odot$ yr^{-1}, we can estimate the radio contribution from star formation, using the relation between the SFR and radio flux (e.g., the expression in Sect. 3.2 in Greiner et al. 2016). After subtracting the star formation contribution, the radio emission from the AGN and/or TDE is obtained at a level of ~31 μJy. As discussed in Sect. 3.1, a persistent harder component from AGN and a variable soft component from TDE are present in the X-ray spectra of J1342. Since only a single-epoch radio observation is available, we cannot tell whether there is a similar radio variability as observed in soft X-rays, which is helpful to identify the radio origin from a TDE. Further observations at radio bands are encouraged to determine whether the radio emission is stable or declining in flux.

3.3. Black hole mass

The BH mass of J1342 is estimated to be $1.1 \times 10^6\ M_\odot$ with an uncertainty of 0.5 dex using the $M - \sigma$ correlation (French et al. 2020). However, Chilingarian et al. (2018) measured its virial BH mass as $9.6 \pm 1.3 \times 10^4\ M_\odot$ using the flux and width of the broad Hα emission from the Magellan/MagE optical spectrum taken on May 30, 2017, which is ~16 years after the flare. Assuming the host-subtracted radio emission originates from a persistent AGN, we can also estimate the BH mass, using the fundamental plane of BH accretion, an empirical correlation of the mass of a BH, its radio luminosity, and its 2–10 keV band power-law continuum luminosity (Gültekin et al. 2014). The BH

mass estimated from this correlation is $4.3 \times 10^5\,M_\odot$, with an uncertainty of 0.8 dex. Besides the intrinsic scatter, the low luminosity of J1342 makes the correction for radio contamination from host emission uncertain. Therefore, BH mass estimation from the fundamental plane should be treated with caution.

Considering the scatter of $M-\sigma$ correlation at low BH mass ($<10^6\,M_\odot$) is very large (Kormendy & Ho 2013), the estimated BH mass of J1342 based on this correlation may have large intrinsic uncertainty. The estimation from a fundamental plane correlation has an even large scatter and whether such a correlation is applicable to SMBHs is still under debate (Gültekin et al. 2019). The systematic uncertainty of the broad Hα-based virial estimation for the BH mass is usually within 0.3 dex (Xiao et al. 2011; Dong et al. 2012). Furthermore, the Magellan/MagE spectrum is obtained 16 years after the flare, and it would scarcely be affected by the flare. Based on these reasons, we prefer the BH mass of $9.6 \times 10^4\,M_\odot$ from the broad Hα-based virial estimation, and we consider the values obtained from the other two methods only for a consistency check; these checks support the presence of an intermediate mass BH (IMBH; $10^2\,M_\odot$ < BH mass < $10^5\,M_\odot$) in J1342.

3.4. IMBH-TDE

The X-ray spectral slope and long-term spectral evolution is similar to other thermal X-ray TDEs, for example, RBS 1032. The luminosity decline of RBS 1032 also follows the $t^{-5/3}$ approximation and has a super-soft spectrum ($\Gamma \sim 5$) at its early phase and remains still very soft ($\Gamma \sim 3.4$) 20 years after the discovery (Maksym et al. 2014). The similar X-ray evolution behavior of J1342 suggests it is also a TDE, which is consistent with the previous studies from its transient coronal lines (Wang et al. 2012; Yang et al. 2013) and mid-infrared dust echo (Dou et al. 2016). If so, it would make J1342 one of the long-lived TDEs lasting more than ten years.

The long-lived TDEs have been discovered in several individuals, including RX J1242.6−1119, RX J1624.9+7554, NGC 5905 (Vaughan et al. 2004), RBS 1032 (Maksym et al. 2014), 3XMM J1500+0154 (Lin et al. 2017a), 3XMM J2150−0551 (Lin et al. 2018, 2020), 2XMM J1231+1106 (Lin et al. 2017b), and GSN 069 (Shu et al. 2018), although the later two source is a TDE occurring in an AGN. We collected their X-ray light curves and plotted these in Fig. 2. We note that the $t^{-5/3}$ declines in their very later phase are also discovered in XMM J2150−0551, GSN069, RX J1242.6−1119, and RBS 1032.

Several theoretical models could explain the long-lived TDEs, for example, a long super-Eddington accretion phase, perhaps involving a disrupted object with a large mass (e.g., Lin et al. 2017a), a partially stripped evolved star atmosphere (MacLeod et al. 2012), or later distant circularization (Guillochon & Ramirez-Ruiz 2015; Shiokawa et al. 2015, see also Saxton et al. 2020). For J1342, if adopted the virial BH mass of $\sim 9.6 \times 10^4\,M_\odot$, the X-ray luminosity peak of J1342 estimated from the power-law decline of $t^{-5/3}$ would be one magnitude order larger than its Eddington luminosity ($L_{\rm Edd} = 1.26 \times 10^{38}\,(M_{\rm BH}/M_\odot)\,{\rm erg\,s^{-1}}$). Additionally, these would also have a super-Eddington stage lasting roughly one year in the early stage of outburst.

Chen & Shen (2018) suggest an IMBH-TDE model explains the more than 13 year long-lived TDE 3XMM J2150-0551. These authors predicted that the tidal disruption of a main-sequence star by an IMBH could always be a long-term circularization process, leading a light curve as long as two decades, which still follows the $t^{-5/3}$ decline in a very later phase. We can also explain the later-time X-ray evolution of J1342 with this IMBH-TDE model, as shown in Fig. 2, for example, the tidal disruption of a main-sequence star with mass of 0.1 $M_\odot$, adopting the virial BH mass of $\sim 9.6 \times 10^4\,M_\odot$.

4. Conclusion

X-ray emission was detected in the TDE J1342 from *Swift*/XRT and *XMM-Newton*/pn observations, which is ∼9 and 19 years after the flare. The luminosity of the *XMM-Newton* observation is fainter at $L_{0.3-10\,{\rm keV}} \sim 1.4{\times}10^{41}\,{\rm erg\,s^{-1}}$, compared to the value, $L_{0.3-10\,{\rm keV}} \sim 2.8{\times}10^{41}\,{\rm erg\,s^{-1}}$ of *Swift*. We find, however, that the variation is mostly from the emission in soft X-ray: $L_{0.3-2\,{\rm keV}} \sim 5.2 \times 10^{40}\,{\rm erg\,s^{-1}}$ in *XMM-Newton* observation and $L_{0.3-2\,{\rm keV}} \sim 1.9 \times 10^{41}\,{\rm erg\,s^{-1}}$ in *Swift*. The emission in hard 2–10 keV band is consistent between the two observations.

To infer the nature of the variation we modeled the spectra with two-component models, including one flat hard power law plus one steep power law, or a blackbody component. The flat, hard power-law component could be explained as the persistent AGN activity. We find some TDE evidence as follows:

– The soft component can be well fitted with a steep power law or blackbody model. The spectra is somewhat harder at fading phase of duration years with $\Gamma = 3.7 \pm 0.5$ as obtained from *XMM-Newton*, compared to $\Gamma = 4.8^{+1.2}_{-0.9}$ as obtained with *Swift*, although the spectral slopes are consistent with each other if we consider the uncertainties. In a blackbody modeling the inferred temperature is $kT = 78^{+20}_{-17}$ eV, and $kT = 90^{+16}_{-14}$ eV in the spectra of *Swift* and *XMM-Newton*, separately.
– The 0.3–2 keV band luminosity of the soft component fades from 1.8×10^{41} to $3.7 \times 10^{40}\,{\rm erg\,s^{-1}}$ in ∼10 years. The declination of the luminosity is well fitted with $t^{-5/3}$ model.
– The estimated peak luminosity of the flare is $\sim 10^{44}\,{\rm erg\,s^{-1}}$ with an assumption of $t^{-5/3}$ declination.

Therefore, the soft X-ray spectral shape and luminosity evolution further support that J1342 is a TDE candidate, which justifies the previous studies with transient coronal lines (Wang et al. 2012; Yang et al. 2013) and mid-infrared dust echo (Dou et al. 2016). Furthermore, if the BH mass of $\sim 9.6 \times 10^4\,M_\odot$ estimated from the Hα emission in the 16 year later-time optical spectrum is reliable, J1342 would be a long-lived IMBH-TDE candidate.

Acknowledgements. We would like to thank the anonymous referee and the editor Prof. Sergio Campana for the suggestions and comments that greatly improved the paper. This work is supported by Joint Research Foundation in Astronomy (U1731104, U1731109, U2031106) under cooperative agreement between the NSFC and the CAS, Chinese Science Foundation (NSFC-11833007, 11822301, 11733001). We acknowledge the science research grants from the China Manned Space Project with No. CMS-CSST-2021-A05 and CMS-CSST-2021-B11. L.M.D. and J.S.H. also acknowledge the support from the Key Laboratory for Astronomical Observation and Technology of Guangzhou, the Astronomy Science and Technology Research Laboratory of Department of Education of Guangdong Province, the opening fund of CAS Key Laboratory of Galaxy Cosmology (No.18010201).

References

Ai, Y., Yuan, W., Zhou, H., Wang, T., & Zhang, S. 2010, ApJ, 727, 31
Auchettl, K., Guillochon, J., & Ramirez-Ruiz, E. 2017, ApJ, 838, 149
Bade, N., Komossa, S., & Dahlem, M. 1996, A&A, 309, L35
Burrows, D. N., Hill, J., Nousek, J. A., et al. 2005, Space Sci. Rev., 120, 165
Cannizzo, J., & Gehrels, N. 2009, ApJ, 700, 1047
Chen, J.-H., & Shen, R.-F. 2018, ApJ, 867, 20

Chilingarian, I. V., Katkov, I. Y., Zolotukhin, I. Y., et al. 2018, ApJ, 863, 1
Dong, X.-B., Ho, L. C., Yuan, W., et al. 2012, ApJ, 755, 167
Dou, L., Wang, T.-G., Jiang, N., et al. 2016, ApJ, 832, 188
Dou, L., Wang, T., Yan, L., et al. 2017, ApJ, 841, L8
Evans, C. R., & Kochanek, C. S. 1989, ApJ, 346, L13
French, K. D., Wevers, T., Law-Smith, J., Graur, O., & Zabludoff, A. I. 2020, Space Sci. Rev., 216, 1
Gehrels, N., Chincarini, G., Giommi, P., et al. 2004, ApJ, 611, 1005
Gliozzi, M., & Williams, J. K. 2020, MNRAS, 491, 532
Greiner, J., Michałowski, M. J., Klose, S., et al. 2016, A&A, 593, A17
Guillochon, J., & Ramirez-Ruiz, E. 2015, ApJ, 809, 166
Gültekin, K., Cackett, E. M., King, A. L., et al. 2014, ApJ, 788, L22
Gültekin, K., King, A. L., Cackett, E. M., et al. 2019, ApJ, 871, 80
Hills, J. G. 1975, Nature, 254, 295
Jiang, N., Dou, L., Wang, T., et al. 2016, ApJ, 828, L14
Jiang, N., Wang, T., Yan, L., et al. 2017, ApJ, 850, 63
Jiang, N., Wang, T., Mou, G., et al. 2019, ApJ, 871, 15
Jiang, N., Wang, T., Dou, L., et al. 2021, ApJS, 252, 32
Jonker, P., Stone, N., Generozov, A., van Velzen, S., & Metzger, B. 2020, ApJ, 889, 166
Kalberla, P. M., Burton, W., Hartmann, D., et al. 2005, A&A, 440, 775
Komossa, S. 2015, J. High Energy Astrophys., 7, 148
Komossa, S., & Bade, N. 1999, A&A, 343, 775
Komossa, S., Zhou, H., Wang, T. G., et al. 2008, ApJ, 678, L81
Kormendy, J., & Ho, L. C. 2013, ARA&A, 51, 511
Lamastra, A., Bianchi, S., Matt, G., et al. 2009, A&A, 504, 73
Lin, D., Godet, O., Ho, L. C., et al. 2017a, MNRAS, 468, 783
Lin, D., Guillochon, J., Komossa, S., et al. 2017b, Nat. Astron., 1, 0033
Lin, D., Strader, J., Carrasco, E. R., et al. 2018, Nat. Astron., 2, 656
Lin, D., Strader, J., Romanowsky, A. J., et al. 2020, ApJ, 892, L25
Lu, W., Kumar, P., & Evans, N. J. 2016, MNRAS, 458, 575
Lodato, G., & Rossi, E. M. 2011, MNRAS, 410, 359
MacLeod, M., Guillochon, J., & Ramirez-Ruiz, E. 2012, ApJ, 757, 134
Maksym, W. P., Lin, D., & Irwin, J. A. 2014, ApJ, 792, L29
Mineo, S., Gilfanov, M., & Sunyaev, R. 2012, MNRAS, 426, 1870
Park, T., Kashyap, V., Siemiginowska, A., et al. 2006, ApJ, 652, 610
Phinney, E. S. 1989, in Manifestations of a Massive Black Hole in the Galactic Center, ed. M. Morris (Dordrecht: Kluwer), IAUSymp., 136, 543
Rees, M. J. 1988, Nature, 333, 523
Saxton, R., Komossa, S., Auchettl, K., & Jonker, P. 2020, Space Sci. Rev., 216, 1
Shiokawa, H., Krolik, J. H., Cheng, R. M., et al. 2015, ApJ, 804, 85
Shu, X., Wang, S. S., Dou, L., et al. 2018, ApJ, 857, L16
Vaughan, S., Edelson, R., & Warwick, R. 2004, MNRAS, 349, L1
van Velzen, S., Mendez, A. J., Krolik, J. H., & Gorjian, V. 2016, ApJ, 829, 19
Wang, T.-G., Zhou, H.-Y., Wang, L.-F., Lu, H.-L., & Xu, D. 2011, ApJ, 740, 85
Wang, T.-G., Zhou, H.-Y., Komossa, S., et al. 2012, ApJ, 749, 115
Wang, T., Yan, L., Dou, L., et al. 2018, MNRAS, 477, 2943
Xiao, T., Barth, A. J., Greene, J. E., et al. 2011, ApJ, 739, 28
Yang, C.-W., Wang, T.-G., Ferland, G., et al. 2013, ApJ, 774, 46